Bioorganic & Medicinal Chemistry 18 (2010) 7611–7620

Contents lists available at ScienceDirect

Bioorganic & Medicinal Chemistry

journal homepage: www.elsevier.com/locate/bmc

Small molecule peptidomimetic inhibitors of importin α/β mediated nuclear transport

Géza Ambrus [a], Landon R. Whitby [b], Eric L. Singer [a], Oleg Trott [c], Euna Choi [a], Arthur J. Olson [c], Dale L. Boger [b], Larry Gerace [a,*]

[a] Department of Cell Biology, The Scripps Research Institute, 10550 N Torrey Pines Rd., La Jolla, CA 92037, USA
[b] Department of Chemistry, The Scripps Research Institute, 10550 N Torrey Pines Rd., La Jolla, CA 92037, USA
[c] Department of Molecular Biology, The Scripps Research Institute, 10550 N Torrey Pines Rd., La Jolla, CA 92037, USA

ARTICLE INFO

Article history:
Received 9 July 2010
Revised 17 August 2010
Accepted 18 August 2010
Available online 21 August 2010

Keywords:
High content screening
Nucleocytoplasmic transport
Importin β
Small molecule inhibitor
Peptidomimetics

ABSTRACT

Nucleocytoplasmic transport of macromolecules is a fundamental process of eukaryotic cells. Translocation of proteins and many RNAs between the nucleus and cytoplasm is carried out by shuttling receptors of the β-karyopherin family, also called importins and exportins. Leptomycin B, a small molecule inhibitor of the exportin CRM1, has proved to be an invaluable tool for cell biologists, but up to now no small molecule inhibitors of nuclear import have been described. We devised a microtiter plate based permeabilized cell screen for small molecule inhibitors of the importin α/β pathway. By analyzing peptidomimetic libraries, we identified β-turn and α-helix peptidomimetic compounds that selectively inhibit nuclear import by importin α/β but not by transportin. Structure–activity relationship analysis showed that large aromatic residues and/or a histidine side chain are required for effective import inhibition by these compounds. Our validated inhibitors can be useful for in vitro studies of nuclear import, and can also provide a framework for synthesis of higher potency nuclear import inhibitors.

1. Introduction

In eukaryotes the nuclear envelope (NE[†]) segregates the nucleus from the cytoplasm.[1] Communication between these compartments involves trafficking of macromolecules through large proteinaceous channels that span the NE, called nuclear pore complexes (NPCs).[2,3] The NPC is made up of multiple copies of approximately 30 different proteins, collectively known as nucleoporins. Macromolecular transport through the NPC is mediated by nuclear transport receptors (also called importins and exportins), most of which are members of the β-karyopherin family.[4–6] The nuclear transport receptors in complex with their cargoes bind to repeats of the Phe-Gly (FG) amino acid motif that occur in natively disordered domains of 'FG-nucleoporins' that line the transport channel of the NPC. These interactions enable the receptors to penetrate the NPC and ferry cargoes into and out of the nucleus.[7] The best characterized import receptors are importin β (also known as karyopherin β1) and transportin (or karyopherin β2). The binding of protein cargoes to import receptors is typically mediated by short amino acid stretches in the cargoes, called nuclear localization sequences (NLSs). The binding of cargoes to importin β frequently is mediated by various isotypes of the adaptor importin α, which recognizes the cargo NLS.[6] Although importin β and transportin are structurally similar, they recognize structurally different NLSs. The 'classical' NLS that is recognized by the importin α/β pathway contains one or two short basic amino acid clusters. By contrast, the well-characterized transportin NLS contains the consensus sequence R/H/KX$_{(2-5)}$PY in addition to an upstream basic or hydrophobic motif.[8]

CRM1, also known as exportin-1, is the major karyopherin that exports many cellular proteins from the nucleus to the cytoplasm, typically through binding to a short leucine rich nuclear export sequence (NES) found on cargoes.[9–13] Multiple mechanisms can regulate nuclear trafficking, including anchoring of cargoes in the nucleus or cytoplasm, and exposure or masking of nuclear import and export signals by protein–protein interactions or by posttranslational modifications. A key component of all karyopherin-mediated import and export pathways is the small GTPase Ran, which uses the energy of GTP hydrolysis to specify transport directionality.[14]

The identification of leptomycin B (LMB), the first small molecule inhibitor of CRM1, has greatly facilitated investigation of nucleocytoplasmic transport.[15] LMB has been used in hundreds of studies to uncouple nuclear export from import and to analyze nucleocytoplasmic shuttling proteins. In addition to being an extremely useful research tool, LMB has antibiotic and anti-tumor activities although it is cell-toxic. In addition to LMB, several other small molecule inhibitors targeting CRM1 and nuclear export have

* Corresponding author. Tel.: +1 858 784 8514; fax: +1 858 784 9132.
E-mail address: lgerace@scripps.edu (L. Gerace).

[†] *Abbreviations:* NE, nuclear envelope; NLS, nuclear localization sequence; NPC, nuclear pore complex; NES, nuclear export sequence; LMB, leptomycin B; WGA, wheat germ agglutinin; BSA, bovine serum albumin.

0968-0896/$ - see front matter © 2010 Elsevier Ltd. All rights reserved.
doi:10.1016/j.bmc.2010.08.038

been identified,[16–21] as have been affinity-optimized peptide cargoes that may competitively inhibit the transportin and importin α/β nuclear import pathways.[22–24] However, no small molecule inhibitor of nuclear import has been described up to now (Supplementary Fig. S1).

In this study we report the identification and characterization of small molecules that selectively inhibit importin α/β mediated nuclear import. We identified these compounds by screening peptidomimetic libraries, which previously have proven useful for finding compounds that inhibit protein–protein interactions and functions with IC_{50} values in the nanomolar to low micromolar range.[25–29] We have used a high-content screen involving a modified version of a digitonin permeabilized cell nuclear import assay. This yielded multiple different but related inhibitors, with IC_{50} values for transport inhibition in the 100 μM range, only ca. 100-fold less potent than the multivalent macromolecular inhibitor wheat germ agglutinin (WGA). Some of these compounds may have substantially stronger binding affinities for individual nuclear transport factors than reflected by their IC_{50} values, and could be useful for future investigations of the nuclear transport machinery. They also could provide the basis for development of more potent import inhibitors.

2. Results

2.1. Adaptation of the nuclear import assay to 96-well plate format

We carried out screening of peptidomimetic libraries using a permeabilized cell nuclear import assay, which involved incubation of digitonin-permeabilized cells with a fluorescently labeled import cargo and exogenous cytosol as a source of nuclear transport factors (including importins α/β, transportin, and Ran), followed by cell washing and fixation. The accumulation of cargo in the nucleus was determined by light microscopy with automated image acquisition, which allowed analysis of hundreds of cells for each data point. Decrease in nuclear accumulation of fluorescently labeled cargo molecule was the readout for transport inhibition in the primary screen.

The adherent cell lines described by Adam et al. in the original nuclear transport assay were not suitable for screening with 96-well plates, as they were released from the plates due to the digitonin treatment followed by the washing steps (Fig. 1A).[30] We examined multiple cell lines to identify ones suitable for screening, including HaCaT, Cos-7, CV1, NIH 3T3, HeLa, NRK, FGM. We found that only two of these cell lines, FGM and HaCaT, remained reproducibly attached to plate wells by the end of the assay under optimal conditions (data not shown, and below). For screening we have chosen the FGM cell line, a metastatic variant of a pancreatic carcinoma cell line with a relatively uniform nuclear morphology (Fig. 1B).[31] In the presence of GTP, Alexa555 labeled SV40 T antigen NLS peptide conjugated bovine serum albumin cargo (Alexa555-BSA-NLS) was efficiently imported into the nucleus, whereas in the presence of GMP-PNP, an unhydrolyzable GTP analogue nuclear import was inhibited, as expected. The retention of FGM cells attached to the assay wells was enhanced by using precoated multiwell plates, such as Nunc CC^2 coated plates or Greiner poly-D-Lys coated plates. The initial cell seeding density also was a critical factor, and 40,000 cells/well proved to be optimal under our conditions. Edge effects were effectively eliminated by incubating the seeded plates for 1 h at room temperature before transferring them to a CO_2 incubator.[32] Cytosol and Alexa555-BSA-NLS concentrations, as well as incubation times were optimized, and the assay exhibited small well-to-well, plate-to-plate and day-to-day variations. To further confirm the validity of our assay we have tested the concentration dependence for transport inhibition by WGA, a known macromolecular inhibitor of nuclear import.[33] The dose–response curve showed a good fit and resulted in consistent IC_{50} values across experiments (Fig. 1C).

2.2. Screening of 29,067 compounds in the form of compound mixtures

A library of 29,067 peptidomimetic small molecules designed to inhibit protein–protein interactions was screened in the permeabilized cell nuclear import assay and subjected to a series of validation steps (Fig. 2A). The library contained single compounds as well as mixtures with typically 10–20 compounds and occasionally up to 100 compounds.[25] Screening concentrations of DMSO were kept at a constant 1%, and due to varying stock concentrations for separate sublibraries, the total compound/compound mixture concentrations ranged from 10 μm to 500 μM, with final individual compound concentrations never exceeding 25 μM. In the primary

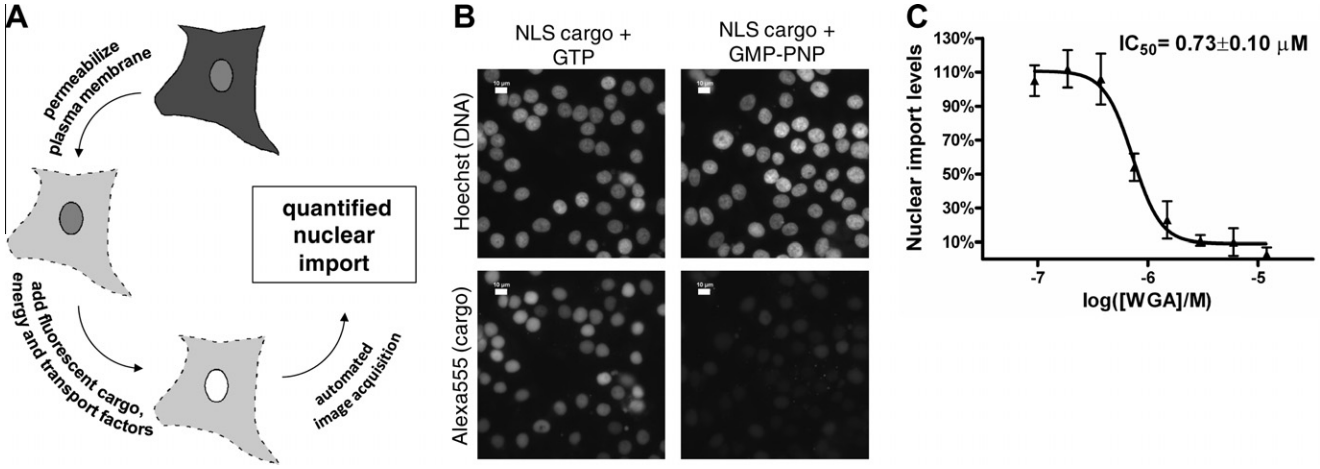

Figure 1. Permeabilized cell nuclear import assay adapted to 96-well plate format. (A) Schematic diagram of permeabilized cell nuclear import assay. Soluble cytosolic components are released after the plasma membrane is perforated by the glycoside digitonin, which leaves the NE and ER membranes intact. An ATP regenerating system, GTP, nuclear transport factors and labeled cargo is added exogenously. The fluorescence accumulated in the nucleus is quantified by light microscopy. (B) Fluorescence microscopy images of permeabilized cells following importin α/β mediated nuclear import. Negative control wells contained GTP and for positive control wells, GMP-PNP was added to achieve complete inhibition of import. Nuclei were stained with Hoechst 33342, and the DNA dye and Alexa555-BSA-NLS cargo were visualized after cell fixation. Scale bar is 10 μm. (C) Dose–response curve of wheat germ agglutinin (WGA), a well-characterized protein inhibitor of nuclear import, as measured in the permeabilized cell nuclear transport assay.

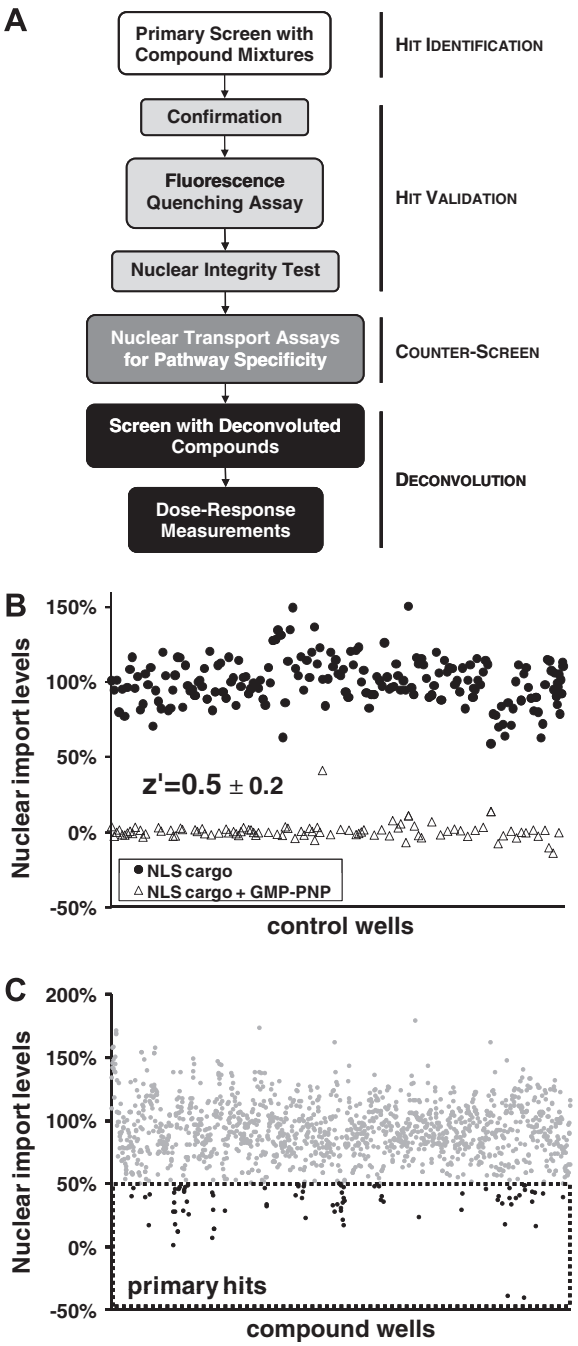

Figure 2. Hit identification and validation. (A) Flowchart for the identification and validation of nuclear import inhibitors of the importin α/β pathway from compound mixtures. (B) Relative nuclear import values of a compilation of negative and positive control wells taken from all of the plates screened (10 negative control wells and 6 positive control wells per plate). The average z' factor derived from the primary screens was 0.5 ± 0.2. (C) Relative nuclear import levels of screened compound mixtures. Compound mixtures with over 50% inhibition were considered primary hits and are highlighted in black.

screen, each plate contained ten negative control replicates, in which DMSO was added in lieu of the compounds, and six positive controls replicates, in which GMP-PNP was added to a 2 mM final concentration to inhibit nuclear import of the NLS cargo by blocking GTP hydrolysis by Ran (Fig. 1B).[34] A compilation of average fluorescence intensity values from individual control wells was used to calculate the z′ factor values for the primary screen (Fig. 2B). Z′ factor values are descriptive of the robustness of an assay and were around 0.5 in our case indicative of an excellent assay.[35] We considered compounds or compound mixtures primary hits if the average nuclear import levels from the respective wells were below 50% of the negative control value (Fig. 2C). Our primary screen returned 65 such primary hits.

2.3. Validation of primary hits

The primary hits all came from compound mixtures of two classes of peptidomimetics: β-turn mimetics and α-helix mimetics (Supplementary Fig. S7). Each of these compound mixtures contained 20 structurally related compounds. The primary hits were rescreened three independent times at 500 μM total compound concentrations (25 μM for each compound). Compound mixtures that gave an average level of nuclear import less than 50% were considered confirmed hits and were further tested to exclude possible artifacts (Fig. 2A). One potential artifact is quenching of the Alexa555 fluorophore present on the cargo molecule by a particular compound. This would cause a loss of fluorescence signal from cargo and could lead to the false conclusion that nuclear import was inhibited. To eliminate such compounds, fluorescence intensities of the nuclear import reaction mixtures containing the fluorescent cargo plus compounds were measured using a benchtop fluorimeter. Three of the compound mixtures caused fluorescence quenching of the Alexa555 dye, and were eliminated from further analysis.

A second potential artifact could be caused by disruption of the permeability barrier of the NE upon exposure to certain types of compounds, which might allow release of fluorescent cargo molecule from the nucleus during the washing steps or during the nuclear import reaction. Once again this could be mistaken for nuclear import inhibition due to the loss of intranuclear signal. To test for such effects, an anti-lamin A/C antibody was included in the nuclear import reaction, and was detected by immunofluorescence microscopy after the completion of the reaction, cell washing and fixation. The anti-lamin A/C antibody, which is too large to diffuse across the NE, only yields nonspecific cytoplasmic background when the NE is intact. However, when the NE integrity is compromised (e.g., by detergents, Fig. 3A, lower middle panel), the antibody diffuses into the nucleus and binds to the lamina, which lines the inner nuclear membrane, leading to a characteristic nuclear rim staining. Two compound mixtures were eliminated from analysis by this validation test (58 E9 shown in Fig. 3A, right panel). The final number of compound mixtures with confirmed inhibitory effects and without detectable artifacts was 46 (Supplementary Fig. S5).

2.4. Counter-screen with M9 cargo identifies compound mixtures that also inhibit transportin mediated nuclear import

To assess the import receptor specificity of inhibition by the 46 compound mixtures, we subjected them to a transport assay to measure transportin-mediated import (Fig. 3B). Instead of the importin α/β specific cargo (Alexa555-BSA-NLS), we used a fluorescently labeled GST fusion of the M9 sequence of hnRNP A1 (Alexa555-GST-M9), a well-described NLS for transportin.[8] The 46 compound mixtures were screened three independent times at 500 μM total compound concentrations (25 μM for each compound). Most of these mixtures showed no significant inhibition of transportin mediated nuclear import, but four of the mixtures did significantly inhibit import of the M9 cargo as well (to less than 50% of control) (Supplementary Fig. S5). These could act by blocking a component common to the two import receptor pathways, such as components of the Ran system. The remaining 42 compound mixtures, which selectively inhibited the importin α/β pathway by our criteria, included 16 β-turn mimetics and 26 α-helix mimetics (Figs. 4A and 5A, Supplementary Figs. S5 and S6).

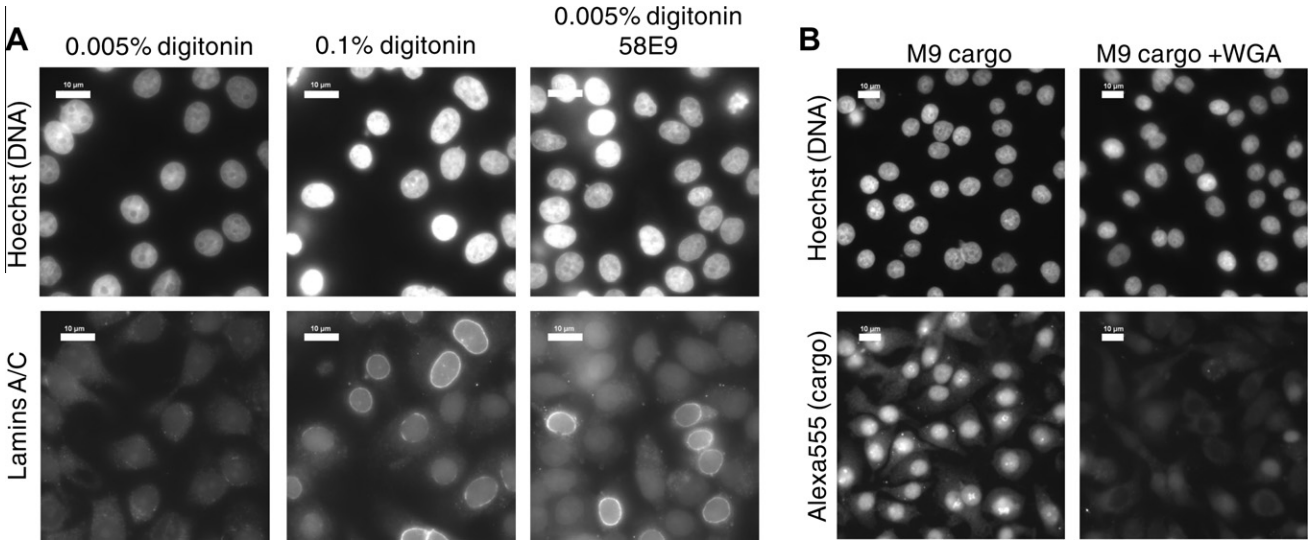

Figure 3. Counter-screen for pathway specificity. (A) Nuclear integrity test of confirmed hits. Control wells were either treated with 0.005% digitonin permeabilizes the plasma membrane but leaves the NE intact, or with 0.1% digitonin that permeabilizes both. Confirmed hits were incubated with cells permeabilized with 0.005% digitonin together with anti-lamins A/C. Immunofluorescence using antibodies against lamins A/C detects cells where the NE integrity is breached, as seen by strong nuclear rim labeling. Only a nonspecific 'haze' of cytoplasmic background was obtained in cells with intact nuclei. Compounds such as 58E9 (right panels) were eliminated from further investigation. Scale bar is 10 μm. (B) Fluorescence microscopy images of permeabilized cells following transportin mediated nuclear import. Positive control wells contained WGA to inhibit import. Nuclei were stained with Hoechst 33342 and Alexa555-GST-M9 cargo was visualized directly. Scale bar is 10 μm.

Although these compound mixtures did not detectably inhibit import of the M9 cargo with our conditions, it is possible that they could affect this pathway at higher concentrations. However, we were unable to test this, because of the need to keep the DMSO concentration at or below 1%. Validated hits that had no detectable inhibition of transportin mediated import at 500 μM total concentration were titrated to 50 μM and still showed statistically significant inhibition of importin α/β mediated nuclear import, indicating an at least 10× selectivity of importin α/β pathway inhibition over transportin pathway inhibition (data not shown).

2.5. Structure–activity relationship analysis of the compound mixtures

The library construction of β-turn mimetic (Whitby, L.R., Ando, Y., et al. soon to be published results) and α-helix mimetic compound mixtures covered all possible combinations of the 20 side chains.[36] This provided a straightforward opportunity for structure–activity relationship (SAR) analysis from our primary screening data. Compounds from both classes were tripeptide mimetics and contained variable positions that were substituted with 20 different side chains (Supplementary Fig. S2). For the α-helix mimetics, all possible $20 \times 20 \times 20 = 8000$ compounds were synthesized in the form of 400 compound mixtures where each mixture contained specific R_i and R_{i+4} groups and an equimixture of the 20 side chains in position R_{i+7} (Fig. 5A). Similarly, all possible β-turn mimetic compounds were synthesized in the form of 20 compound mixtures, but due to the C_2 symmetry present in the scaffold, the total number of mixtures was 210 instead of 400 (Fig. 4A, Supplementary Figs. S3 and S4).

All importin α/β selective, β-turn mimetic hits with the exception of one compound mixture contained at least one aromatic side chain in position R_{i+2}/R_{i+3} (R_{i+2} and R_{i+3} are interchangeable due to C_2 symmetry) and in eight out of the 16 cases, the other side chain also was an aromatic residue (Fig. 4A). Another prevalent residue was histidine, with a total number of five occurrences among the inhibitor mixtures. We grouped these compound mixture hits into two classes (Fig. 4A). All hits that contained at least one His residue formed Class 1 and the remaining hits with at least 1 aromatic side chain were listed as Class 2 compounds. In order to further investigate the potentially dominant roles of certain side chains in the inhibition by the β-turn mimetics, we took the summed average over the 20 mixtures containing a specified side chain substituent in the R_{i+2}/R_{i+3} position (Fig. 4B). This analysis revealed further that among the aryl side chains the bicyclic aromatics Trp and Nap were favored, with Trp by far being the dominant side chain for achieving inhibition. Furthermore, the basic side chains His and Lys also showed significant activity, with the His being second only to Trp. Not surprisingly, the most potent mixture contained both Trp and His at the R_{i+2}/R_{i+3} positions (Supplementary Figs. S9 and S10).

Although the α-helix mimetics that selectively inhibited importin α/β mediated nuclear import were structurally more varied than the β-turn mimetic hits, aromatic and His residues again played key roles in inhibition (Fig. 5A). Analogous to the β-turn mimetics, we classified the 10 members that contained a His side chain as Class 1 compounds, while the remaining 16 members which contained an aromatic residue were grouped as Class 2 compounds. Interestingly, when both R_i and R_{i+4} positions are occupied by aromatic groups, HoPhe is a preferred side chain in position R_i of the hits, whereas the structure of the aromatic residue in position R_{i+4} is less restricted (Fig. 5A). Bulky aliphatic groups appear at both R_i and R_{i+4} of the identified inhibitors, with Leu and Ile most prevalent in position R_i of Class 2 hits, whereas Abu, Val, and Leu are found in combination with His in Class 1 (Fig. 5A). The average inhibitory positional analysis (described above for β-turn mimetics) underscored the importance of the aromatic and His residues for inhibition by the α-helix mimetics (Fig. 5B and C). For position R_i, the unsubstituted aromatics Nap and HoPhe showed the greatest activity across their respective 20 mixtures, with His and the small aliphatic Abu also displaying strong effects (Fig. 5B). For R_{i+4}, the mixtures with a His side chain at this position displayed the greatest average% inhibition (Fig. 5C).

2.6. Deconvolution of selected hits identifies individual inhibitor structures

To identify the compounds active in selectively inhibiting importin α/β mediated nuclear import, we chose 3 validated

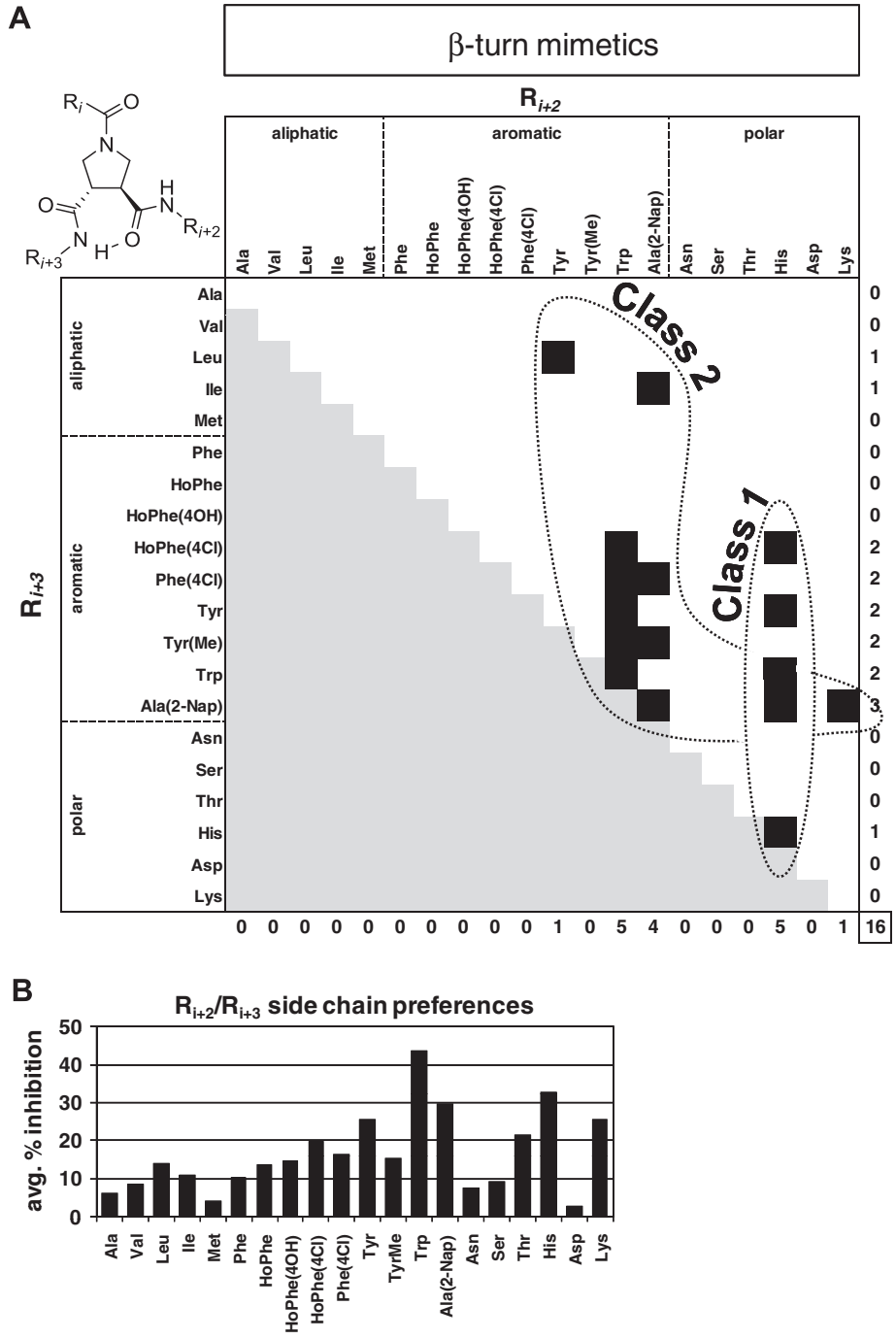

Figure 4. Structural features and activity of β-turn mimetic compound mixtures. (A) Scaffold structure of β-turn mimetics and classification of β-turn mimetic compound mixture inhibitors of importin α/β mediated nuclear import. Each β-turn mimetic compound mixture contains a specific R_{i+2} and R_{i+3} group and a mixture of 20 different structures at the R_i position. Due to the scaffold's C_2 symmetry the R_{i+2} and R_{i+3} groups are interchangeable. Confirmed and validated β-turn mimetic compound mixture inhibitor hits are represented by a black square on the heat map. Redundant structures resulting from the scaffold's C_2 symmetry are in light gray. Please, refer to Supplementary Figure S2 for side chain nomenclature. (B) Average% inhibition over the 20-compound mixtures of the complete β-turn mimetic library, which contain the specified side chain in the R_{i+2}/R_{i+3} position (the average of all 20 variations in the R_{i+3}/R_{i+2} position which contain the specified R_{i+2}/R_{i+3} side chain fixed).

20-compound mixtures and synthesized all their constituent individual compounds separately (60 compounds in total). In addition, we also deconvoluted two compound mixtures from each of the two libraries that showed inhibition of both transportin dependent and importin α/β dependent nuclear import (80 compounds in total). Considering that the original compound mixtures that were screened at 500 μM total concentration contained structurally similar compounds that could all potentially contribute to nuclear import inhibition, we decided to test the deconvoluted compounds at 500 μM, as well, in the nuclear import assay for inhibition of Alexa555-BSA-NLS nuclear import (Supplementary Fig. S8). For the β-turn mimetics, the screening of the 20 individual compounds in the best performing mixture (Trp-His) revealed that aryl substituents were highly preferred at the R_i position, with virtually all compounds containing an aryl substituent showing significantly greater inhibition versus those with non-aryl substituents

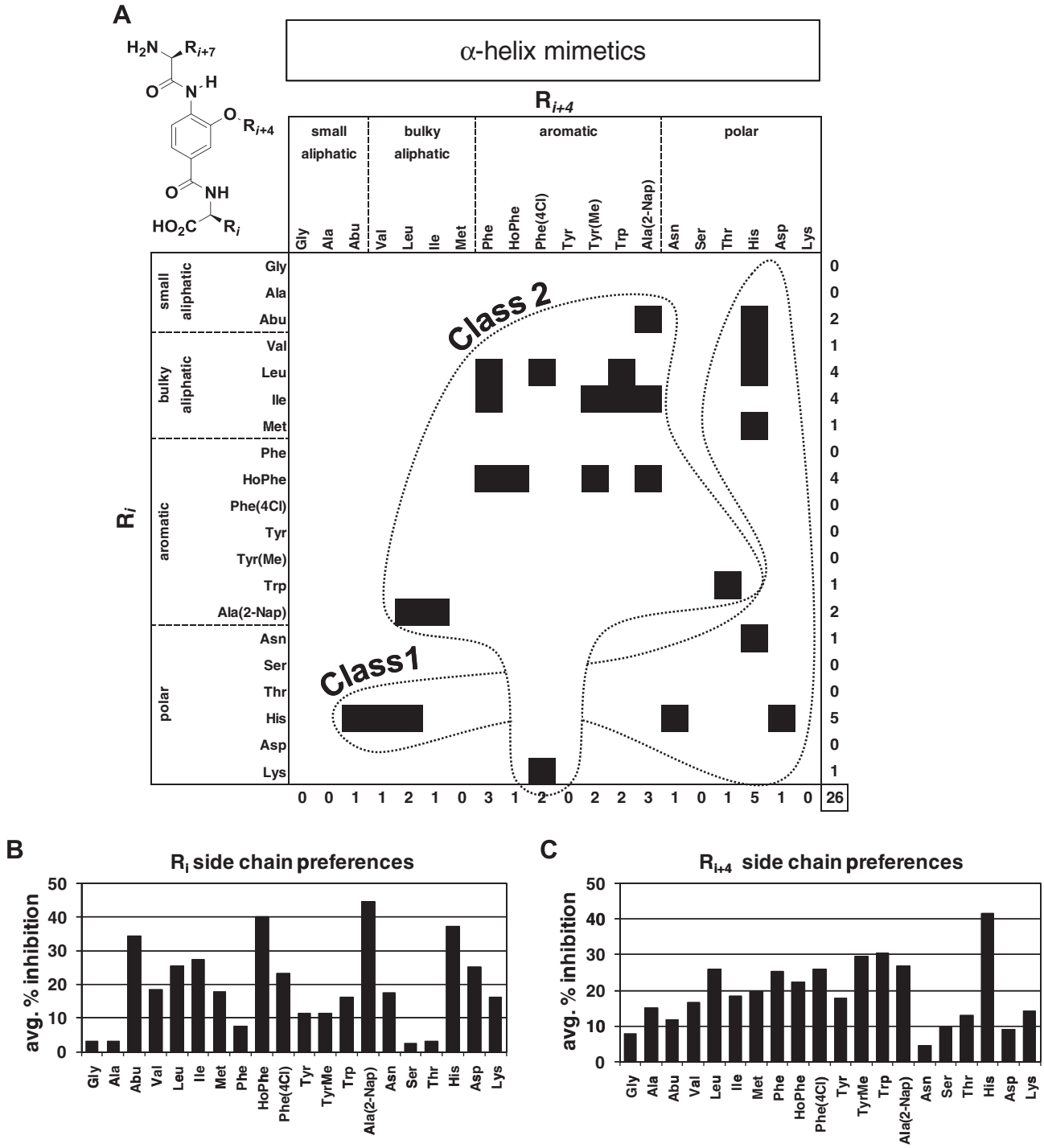

Figure 5. Structural features and activity α-helix mimetic compound mixtures. (A) Scaffold structure of α-helix mimetics and classification of α-helix mimetic compound mixture inhibitors of importin α/β mediated nuclear import. Each α-helix mimetic compound mixture contains a specific R_i and R_{i+4} group and a mixture of 20 different structures at the R_{i+7} position. Confirmed and validated α-helix mimetic compound mixture inhibitor hits are represented by a black square on the heat map. Please, refer to Supplementary Figure S2 for side chain nomenclature. (B) Average% inhibition over the 20-compound mixtures of the complete α-helix mimetic library which contain the specified side chain at the R_i position (the average of all 20 variations of R_{i+4} containing the specified R_i fixed). (C) Average% inhibition over the 20 mixtures of the α-helix mimetic library, which contain the specified side chain at the R_{i+4} position (the average of all 20 variations of R_i containing the specified R_{i+4} fixed).

(Supplementary Fig. S10). Among the aryl side chains, Trp, Nap, and Tyr derivatives (Tyr, TyrMe, HoPhe(4OH)) performed the best (Supplementary Fig. S10).

From the α-helix mimetic deconvolutions, we identified and characterized the most potent inhibitor, 58H5-6 (R_i = HoPhe, R_{i+4} = Phe, R_{i+7} = Ile, Fig. 6C). At as low as 31 μM concentration 58H5-6 detectably inhibited the accumulation of Alexa555-BSA-NLS, but even at 500 μM compound concentration it gave no inhibition of Alexa555-GST-M9, indicating an at least 15-fold selectivity of inhibition of the importin α/β over transportin mediated nuclear trafficking in vitro (Fig. 6A and B). Dilution series of 58H5-6 gave highly reproducible dose–response curves of nuclear import inhibition of Alexa555-BSA-NLS cargo accumulation in the nucleus. These yielded an IC_{50} value of 106 μM for 58H5-6 in the

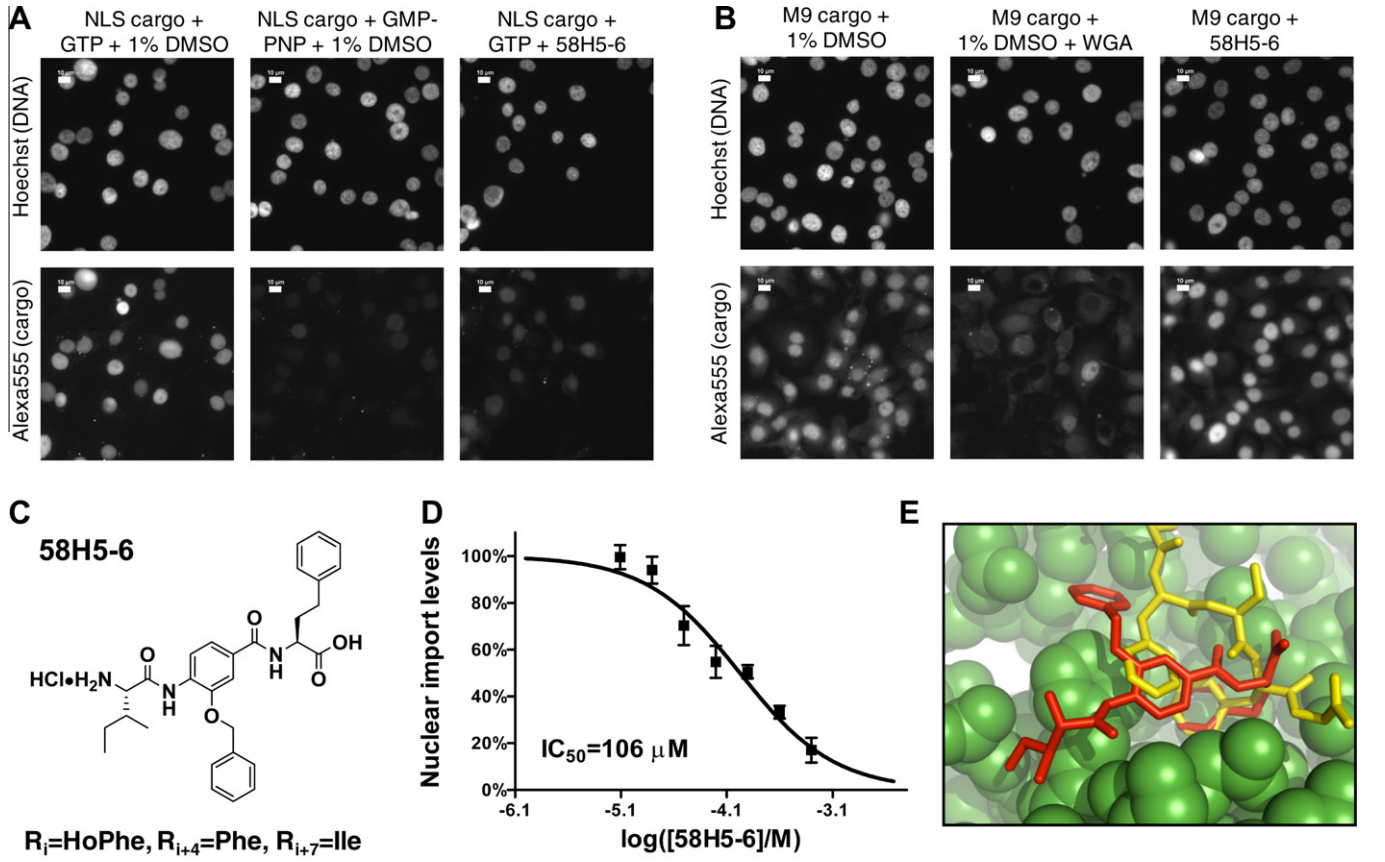

Figure 6. Structure and activity of compound 58H5-6. (A) Nuclear import of Alexa555-BSA-NLS cargo in the cell permeabilized nuclear import assay in the presence of 1% DMSO (negative control), 1% DMSO and 2 mM GMP-PNP (positive control) or 500 μM 58H5-6. Scale bar is 10 μm. (B) Nuclear import of Alexa555-GST-M9 cargo in the cell permeabilized nuclear import assay in the presence of 1% DMSO (negative control), 1% DMSO and 1 mg/ml WGA (positive control) or 500 μM 58H5-6. Scale bar is 10 μm. (C) Structure of 58H5-6. (D) Dose–response curve of 58H5-6 in the cell permeabilized nuclear import assay using the importin α/β cargo Alexa555-BSA-NLS. (E) The thermodynamically most stable conformation of 58H5-6 docked into an FxFG binding site on importin β. The 58H5-6 inhibitor (red) docked to importin β (green) is superimposed on the crystallographic structure of an FxFG peptide fragment (yellow).

permeabilized cell nuclear import assay (Fig. 6D). We used surface plasmon resonance to analyze whether 58H5-6 affects the binding of importin β to the IBB domain of importin α, to RanGTP or to the FG-domain of Nup153, but detected no observable effects (Supplementary Fig. S11). Nor were we able to observe any in vivo inhibitory effect of 58H5-6 on the importin α/β pathway by analysis of the nucleocytoplasmic shuttling protein GFP-NFAT (Supplementary Fig. S12).

2.7. Molecular docking reveals a potential binding site of 58H5-6 on importin β

The structure of 58H5-6, our most potent nuclear import inhibitor, is superficially similar to FxFG repeats found in nucleoporins. We hypothesized that 58H5-6 might inhibit nuclear import by interacting with FxFG binding pockets on importin β to competitively exclude endogenous FG-nucleoporins. To test the plausibility of this hypothesis, we docked 58H5-6 into the region of a previously determined FxFG binding site in the importin β/FxFG crystal complex using AutoDock Vina.[37,38] From this analysis, we found that 58H5-6 docks into this pocket without any steric clashes. Moreover, when 58H5-6 is docked in a fully flexible mode to the rigid FxFG binding pocket of importin β, the thermodynamically most stable conformation among the various predicted binding modes is one that is very similar to that of the FxFG peptide (Fig. 6E). In this conformation, the buried phenyl group (R_i = HoPhe) and the central benzene group of the 58H5-6 inhibitor align well with the phenylalanine side chains of the FxFG peptide. This analysis supports the possibility that 58H5-6 may act by binding to FxFG binding pockets of importin β.

3. Discussion

This work, along with another recent study from our laboratory,[39] describes the first small molecule inhibitors of importin α/β mediated nuclear import. To identify inhibitors in the study described here, we have adapted a permeabilized cell nuclear import assay, pioneered in our laboratory two decades ago, to a 96-well plate format. This in vitro setup provides some advantages over previously described in vivo nuclear import screens that monitor the nuclear localization of endogenous or transfected proteins in cells.[40,41] First, since the cargo consists of an ectopic NLS conjugated to or fused to a carrier protein, it is not subject to regulation that may occur for a normal cellular protein (involving NLS activation or protein anchoring). Thus, our assay is more likely to reveal hits that directly target components of the nuclear transport machinery rather than other regulatory elements such as kinases. Second, cell-impermeable inhibitors are not discarded in the screening process since the assay involves permeabilized cells. Compound properties such as cell-permeability can later be optimized by structure scans or selective chemical modifications that remove or suitably replace charged functional groups and/or enhance lipophilicity. Moreover, the permeabilized cell assay can be used to analyze hits emerging from other in vitro protein based assays, which screen for inhibitors of a specific protein–protein

interaction or for binding of a compound to a member of the nuclear transport machinery, such as our recent screen for importin β binding compounds.

Another important feature of our screen was its focus on peptidomimetic libraries, which have proven useful for obtaining inhibitors of protein–protein interactions. Throughout the nuclear import cycle from cargo binding to recycling of the receptor, at least 6 types of protein–protein interaction govern nuclear transport but only one enzymatic reaction occurs, the hydrolysis of GTP by Ran. We obtained over 60 independent compound mixtures with significant inhibitory activity by screening with a cargo for the importin α/β pathway. All hits identified came from two sublibraries: β-turn and α-helix tripeptide mimetics. In three independent rescreenings of the primary hits, we eliminated compound mixtures that did not reproduce the inhibition, and in two additional tests we excluded false positives that yielded nonspecific effects on the transport signal. This left us with 46 compound mixtures that were specific hits. In an additional counterscreen, we determined that 4 of these confirmed hits inhibited transportin mediated nuclear import as well as importin α/β import. These compounds most probably act on components common to the importin α/β and transportin mediated pathways, such as components of the Ran machinery or certain FG-nucleoporins. Given the high conservation of the nuclear transport machinery among higher eukaryotes,[42–45] it is very likely that all of the above inhibitors—both importin α/β specific and nonspecific ones—are efficacious in all human and most probably in all mammalian cell lines. This hypothesis, however, remains to be tested.

Since both the β-turn and α-helix peptidomimetic sublibraries were constructed to contain all possible combinations of groups representing 20 side chains used in the library synthesis, the correlation of structure with inhibition could be comprehensively characterized. Interestingly, confirmed hits from both sublibraries contained either a histidine or an aromatic residue in one of their two positions. On the one hand, the clustering of specific hits is a validation of our screening and substantiates the structural features of this class of nuclear import inhibitors. On the other hand, the relatively restricted structural diversity of the hits that we obtained was not expected, because of the large number of protein–protein interfaces involved in nuclear protein import that could potentially serve as targets. Thus, our screen may have identified inhibitors of only a subset of these interactions, such as the binding of importin β to nucleoporins. Nucleoporin binding of nuclear transport receptors occurs through FxFG amino acid repeats present in nucleoporins and many of our aromatic residue containing hits may mimic such an FxFG structure, particularly the strongest individual inhibitor we obtained, 58H5-6 (Fig. 6C).

We synthesized individual compounds from a total of seven compound mixtures and rescreened them in our primary assay. A compound from Class 2 of the α-helix peptidomimetic sublibrary, 58H5-6, proved to be the most potent individual compound that inhibited the importin α/β pathway. 58H5-6 showed an IC_{50} value of 106 μM for importin α/β mediated nuclear import in vitro, and no inhibition of transportin mediated nuclear import by 58H5-6 could be detected up to 500 μM. Our docking study confirmed the steric and energetic plausibility of 58H5-6 binding to FxFG pockets on importin β. While this offers an attractive mode of action, i.e. the inhibition of importin β binding to nucleoporins (probably other than Nup153); docking predictions are not guaranteed to reflect physiological processes. The relatively weak IC_{50} value of 58H5-6 may simply be a consequence of the large structural flexibility of importin β[46,47] and/or its multiple, distinct binding pockets for FG repeats,[48] if 58H5-6 indeed acts by inhibiting FG-nucleoporin binding. Although this potency of inhibition may appear modest, it is worth highlighting that this is only approximately 100-fold less potent than the tetravalent macromolecular inhibitor wheat germ agglutinin (WGA). It is also worth noting that larger protein fragments, such as the 211 amino acid long Nup153-FG construct that contains nine FG repeats[49] and the 119 amino acid long Nsp1p derived FF5 construct that contains five FG repeats[50] inhibited in vitro nuclear import at a concentration of 25 μM and 10 μM, respectively. Considering the size of these fragments and the probable avidity effects of the multiple FG repeats, these concentration ranges are in line with the IC_{50} value of 58H5-6. No inhibition of importin α/β mediated nuclear import could be observed in vivo, possibly due to insufficient cell permeability of 58H5-6. We cannot formally rule out an enzymatic activity in cells or medium that modifies the peptidomimetic, although this seems very unlikely. Initial experiments to identify the target of 58H5-6 through a series of surface plasmon resonance tests were unsuccessful. Further chemical modification and optimization of 58H5-6 could lead to a more soluble and/or more potent compound that could facilitate target identification.

In summary, along with a separate very recent study from our laboratory,[39] we have provided the first description of small molecule inhibitors selectively targeting importin α/β mediated nuclear import. We describe the prototype of these inhibitors and offer a hypothesis for mode of action. These compounds could provide the structural basis for the development of higher affinity and/or cell permeable inhibitors in the future.

4. Experimental

4.1. Library construction

The α-helix mimetic and β-turn mimetic libraries are part of a general small-molecule library designed to selectively modulate protein–protein interactions by targeting the three main recognition motifs which mediate protein–protein interactions (α-helix, β-turn, β-strand).[36] The α-helix mimetic library was designed and synthesized as previously described[36] to yield an 8000-member library (20 × 20 × 20) composed of 400 mixtures of 20 structurally related compounds which vary at the N-terminal position. The β-turn mimetic library was constructed around a *trans*-pyrrolidine-3,4-dicarboxamide scaffold, which closely satisfies the geometric constraints provided by a C_α-triplet analysis[51] for the display of triplets of amino acid side chain moieties in a manner similar to a majority of the classes of β-turns (Supplementary Fig. S3). The library was formatted and synthesized as outlined in Supplementary Figure S4 to comprise a 4200-membered library composed of 210 mixtures of 20 structurally related compounds, which vary only at the R_3 position. Notably, all triplet combinations of groups which represent the 20 natural amino acid side chains (or suitable replacements, see Supplementary Fig. S2) are comprehensively represented in the β-turn mimetic library with only 4200 compounds due to the simplifying C_2 symmetry of the *trans*-pyrrolidine-3,4-dicarboxamide scaffold. See Supplementary data for NMR quality control measurements on compound 58H5-6.

4.2. Nuclear import assay

Nuclear import assays using permeabilized cells were carried out as previously described[52] with the following modifications. FGM cells were seeded into poly-D-Lys coated clear bottom 96-well plates (Greiner) at 40,000 cells per well. Plates were left at room temperature for 1 h before transferring them to 37 °C in a CO_2 incubator to avoid edge effects.[32] Forty-eight hours after seeding cells were gently washed three times with transport buffer (20 mM HEPES pH 7.4, 110 mM KOAc, 2 mM $Mg(OAc)_2$, 2 mM DTT, 1 mM EGTA, and 1 μg/ml of each leupeptin, aprotinin, pepstatin) in an automated plate washer (Bio-Rad). Cells were then

permeabilized with 0.005% (50 μg/ml) digitonin in transport buffer for 5 min on ice. Cells were gently washed five times with transport buffer and 50 μl reaction mixtures were added to each well. Reaction mixtures contained compounds at indicated concentrations or equivalent amounts of DMSO, 3 mg/ml HeLa cytosol, 0.5 μM cargo, an ATP regenerating system (0.8 mg/ml creatine phosphate, 10 U/ml creatine phosphokinase, 1 mM ATP), 0.2 mM GTP, in transport buffer. Compounds and compound mixtures dissolved in DMSO were directly diluted 100× into reaction mixtures to yield a 1% DMSO final concentration. For the duration of the nuclear import assay this level of DMSO was still tolerable for cells. Generally, no detectable precipitation of compounds occurred in almost all cases, and the few cases where this was encountered the data points were discarded. Total stock concentrations for individual compounds and compound mixtures ranged from 10 μM to 500 μM. Cytosol, Alexa555 labeled BSA-NLS and GST-M9 cargoes were prepared as described earlier.[52] Wheat germ agglutinin (WGA) was added at 1 mg/ml and GMP-PNP was added at 2 mM to control reaction mixtures to inhibit import reactions. After the addition of reaction mixtures plates were incubated at 30 °C for 30 min. Then the transport reactions were stopped by the addition of ice cold transport buffer and the plates were left on ice for 10 min. Cells were gently washed 10 times with ice cold transport buffer and fixed with 4% formaldehyde in transport buffer for 30 min at room temperature. Fixed cells were washed three times and stained with 10 μg/ml Hoechst 33342 for 10 min at room temperature. Following five washes, phosphate buffer saline (PBS) containing 50% glycerol was added to wells and the plates were kept at 4 °C for a maximum of 2 days until analyzed by fluorescence microscopy.

4.3. Automated image analysis

96-well plates with completed nuclear transport reactions were analyzed on a Leica DMIRE2 fluorescence microscope equipped with an automated stage. Three images were collected with a 40× magnification objective for each well. Images obtained from individual wells were merged post-acquisition and analyzed using Simple PCI software (Compix). A mask was created based on the nuclear space as defined by the Hoechst 33342 dye and was further eroded three passes (~0.3 μM) to exclude fluorescence signals from the nuclear rim. Nuclei that were only partially captured at the edge of the images, as well as fluorescence speckles were discarded. Fluorescence signals coming from cells positioned in close vicinity were separated and assigned to individual nuclei. Cargo fluorescence intensities were then quantified and the average fluorescence intensity per nucleus was calculated. Typically 200–300 nuclei were analyzed per well.

4.4. Nuclear integrity test

The nuclear integrity test was carried out using the conditions of the nuclear import reactions, with the following modifications. Cells were permeabilized by either 0.005% or 0.1% digitonin. Affinity purified antibody directed against lamins A/C was added at 2.5 μg/ml to nuclear import reaction mixtures containing the Alexa555-BSA-NLS cargo. Once the cells were fixed and washed, they were permeabilized with 0.2% Triton X-100 in PBS and blocked with 10% fetal bovine serum in PBS. FITC conjugated secondary antibodies were use to detect the lamin A/C antibody. Samples were analyzed by a Leica DMIRE2 fluorescence microscope.

4.5. Molecular docking

The inhibitor was docked to site 1[37] of chain C from PDB ID 1O6O with the peptide fragment removed. AutoDock Vina 1.1.1[38] was used for docking calculations. The 'search space' was chosen to be an XYZ-coordinates aligned box with 5 Å margins around where the peptide fragment would have been. The rest of the parameters were left at their default values. The receptor was treated as rigid, and the inhibitor fully flexible during docking.

Acknowledgment

This work was supported by NIH Grant R21NS059460 to L.G. and CA078045 to D.B.

Supplementary data

Supplementary data associated with this article can be found, in the online version, at doi:10.1016/j.bmc.2010.08.038.

References and notes

1. D'Angelo, M. A.; Hetzer, M. W. *Cell. Mol. Life Sci.* **2006**, *63*, 316.
2. Terry, L. J.; Shows, E. B.; Wente, S. R. *Science* **2007**, *318*, 1412.
3. Stewart, M. *Nat. Rev. Mol. Cell Biol.* **2007**, *8*, 195.
4. Bednenko, J.; Cingolani, G.; Gerace, L. *Traffic* **2003**, *4*, 127.
5. Cook, A.; Bono, F.; Jinek, M.; Conti, E. *Annu. Rev. Biochem.* **2007**, *76*, 647.
6. Gorlich, D.; Henklein, P.; Laskey, R. A.; Hartmann, E. *EMBO J.* **1996**, *15*, 1810.
7. Rout, M. P.; Aitchison, J. D.; Magnasco, M. O.; Chait, B. T. *Trends Cell Biol.* **2003**, *13*, 622.
8. Lee, B. J.; Cansizoglu, A. E.; Suel, K. E.; Louis, T. H.; Zhang, Z.; Chook, Y. M. *Cell* **2006**, *126*, 543.
9. Fornerod, M.; Ohno, M.; Yoshida, M.; Mattaj, I. W. *Cell* **1997**, *90*, 1051.
10. Fukuda, M.; Asano, S.; Nakamura, T.; Adachi, M.; Yoshida, M.; Yanagida, M.; Nishida, E. *Nature* **1997**, *390*, 308.
11. Neville, M.; Stutz, F.; Lee, L.; Davis, L. I.; Rosbash, M. *Curr. Biol.* **1997**, *7*, 767.
12. Ossareh-Nazari, B.; Bachelerie, F.; Dargemont, C. *Science* **1997**, *278*, 141.
13. Stade, K.; Ford, C. S.; Guthrie, C.; Weis, K. *Cell* **1997**, *90*, 1041.
14. Nachury, M. V.; Weis, K. *Proc. Natl. Acad. Sci. U.S.A.* **1999**, *96*, 9622.
15. Wolff, B.; Sanglier, J. J.; Wang, Y. *Chem. Biol.* **1997**, *4*, 139.
16. Bonazzi, S.; Eidam, O.; Guttinger, S.; Wach, J. Y.; Zemp, I.; Kutay, U.; Gademann, K. *J. Am. Chem. Soc.* **2010**, *132*, 1432.
17. Daelemans, D.; Afonina, E.; Nilsson, J.; Werner, G.; Kjems, J.; De Clercq, E.; Pavlakis, G. N.; Vandamme, A. M. *Proc. Natl. Acad. Sci. U.S.A.* **2002**, *99*, 14440.
18. Mutka, S. C.; Yang, W. Q.; Dong, S. D.; Ward, S. L.; Craig, D. A.; Timmermans, P. B.; Murli, S. *Cancer Res.* **2009**, *69*, 510.
19. Van Neck, T.; Pannecouque, C.; Vanstreels, E.; Stevens, M.; Dehaen, W.; Daelemans, D. *Bioorg. Med. Chem.* **2008**, *16*, 9487.
20. Meissner, T.; Krause, E.; Vinkemeier, U. *FEBS Lett.* **2004**, *576*, 27.
21. Koster, M.; Lykke-Andersen, S.; Elnakady, Y. A.; Gerth, K.; Washausen, P.; Hofle, G.; Sasse, F.; Kjems, J.; Hauser, H. *Exp. Cell Res.* **2003**, *286*, 321.
22. Yang, S. N.; Takeda, A. A.; Fontes, M. R.; Harris, J. M.; Jans, D. A.; Kobe, B. *J. Biol. Chem.* **2010**, *285*, 19935.
23. Cansizoglu, A. E.; Lee, B. J.; Zhang, Z. C.; Fontoura, B. M.; Chook, Y. M. *Nat. Struct. Mol. Biol.* **2007**, *14*, 452.
24. Kosugi, S.; Hasebe, M.; Entani, T.; Takayama, S.; Tomita, M.; Yanagawa, H. *Chem. Biol.* **2008**, *15*, 940.
25. Boger, D. L.; Desharnais, J.; Capps, K. *Angew. Chem., Int. Ed.* **2003**, *42*, 4138.
26. Boger, D. L. *Bioorg. Med. Chem.* **2003**, *11*, 1607.
27. Cheng, S.; Tarby, C. M.; Comer, D. D.; Williams, J. P.; Caporale, L. H.; Myers, P. L.; Boger, D. L. *Bioorg. Med. Chem.* **1996**, *4*, 727.
28. Cheng, S.; Comer, D. D.; Williams, J. P.; Myers, P. L.; Boger, D. L. *J. Am. Chem. Soc.* **1996**, *118*, 2567.
29. Boger, D. L.; Tarby, C. M.; Myers, P. L.; Caporale, L. H. *J. Am. Chem. Soc.* **1996**, *118*, 2109.
30. Adam, S. A.; Marr, R. S.; Gerace, L. *J. Cell Biol.* **1990**, *111*, 807.
31. Shields, D. J.; Niessen, S.; Murphy, E. A.; Mielgo, A.; Desgrosellier, J. S.; Lau, S. K.; Barnes, L. A.; Lesperance, J.; Bouvet, M.; Tarin, D.; Cravatt, B. F.; Cheresh, D. A. *Proc. Natl. Acad. Sci. U.S.A.* **2010**, *107*, 2189.
32. Lundholt, B. K.; Scudder, K. M.; Pagliaro, L. *J. Biomol. Screen.* **2003**, *8*, 566.
33. Yoneda, Y.; Imamoto-Sonobe, N.; Yamaizumi, M.; Uchida, T. *Exp. Cell Res.* **1987**, *173*, 586.
34. Melchior, F.; Paschal, B.; Evans, J.; Gerace, L. *J. Cell Biol.* **1993**, *123*, 1649.
35. Zhang, J. H.; Chung, T. D.; Oldenburg, K. R. *J. Biomol. Screen.* **1999**, *4*, 67.
36. Shaginian, A.; Whitby, L. R.; Hong, S.; Hwang, I.; Farooqi, B.; Searcey, M.; Chen, J.; Vogt, P. K.; Boger, D. L. *J. Am. Chem. Soc.* **2009**, *131*, 5564.
37. Bayliss, R.; Littlewood, T.; Strawn, L. A.; Wente, S. R.; Stewart, M. *J. Biol. Chem.* **2002**, *277*, 50597.
38. Trott, O.; Olson, A. J. *J. Comput. Chem.* **2010**, *31*, 455.
39. Hintersteiner, M.; Ambrus, G.; Bednenko, J.; Schmied, M.; Knox, A.; Gstach, H.; Seifert, J.-M.; Singer, E.; Gerace, L.; Auer, M. *ACS Chem. Biol.* **2010**, in press.
40. Lundholt, B. K.; Linde, V.; Loechel, F.; Pedersen, H. C.; Moller, S.; Praestegaard, M.; Mikkelsen, I.; Scudder, K.; Bjorn, S. P.; Heide, M.; Arkhammar, P. O.; Terry, R.; Nielsen, S. J. *J. Biomol. Screen.* **2005**, *10*, 20.

41. Kwon, Y. J.; Genovesio, A.; Youl Kim, N.; Hi Chul, K.; Jung, S.; David-Watine, B.; Nehrbass, U.; Emans, N. *J. Biomol. Screen.* **2007**, *12*, 621.
42. Goldfarb, D. S.; Corbett, A. H.; Mason, D. A.; Harreman, M. T.; Adam, S. A. *Trends Cell Biol.* **2004**, *14*, 505.
43. Stoffler, D.; Fahrenkrog, B.; Aebi, U. *Curr. Opin. Cell Biol.* **1999**, *11*, 391.
44. Siomi, M. C.; Fromont, M.; Rain, J. C.; Wan, L.; Wang, F.; Legrain, P.; Dreyfuss, G. *Mol. Cell. Biol.* **1998**, *18*, 4141.
45. Rout, M. P.; Aitchison, J. D.; Suprapto, A.; Hjertaas, K.; Zhao, Y.; Chait, B. T. *J. Cell Biol.* **2000**, *148*, 635.
46. Lee, S. J.; Matsuura, Y.; Liu, S. M.; Stewart, M. *Nature* **2005**, *435*, 693.
47. Conti, E.; Muller, C. W.; Stewart, M. *Curr. Opin. Struct. Biol.* **2006**, *16*, 237.
48. Otsuka, S.; Iwasaka, S.; Yoneda, Y.; Takeyasu, K.; Yoshimura, S. H. *Proc. Natl. Acad. Sci. U.S.A.* **2008**, *105*, 16101.
49. Shah, S.; Forbes, D. J. *Curr. Biol.* **1998**, *8*, 1376.
50. Bayliss, R.; Littlewood, T.; Stewart, M. *Cell* **2000**, *102*, 99.
51. Garland, S. L.; Dean, P. M. *J. Comput. Aided Mol. Des.* **1999**, *13*, 469.
52. Cassany, A.; Gerace, L. *Methods Mol. Biol.* **2009**, *464*, 181.